DESIGN AND CONSTRUCTION OF A ONE-PIECE MULTIFUNCTIONAL SMALL SATELLITE BUS STRUCTURE

H. L. McManus*, C. T. Dunn**, and M. Socha***
Massachusetts Institute of Technology and Draper Laboratory
Cambridge MA

Abstract

This paper describes the design and manufacture of a multifunctional space structure. The analytical techniques used in this project included thermal analyses of structures in various earth orbits, determination of structural requirements from optical performance calculations, designing of near zero Coefficient of Thermal Expansion (CTE) laminates, consideration of manufacturing and material variations in design, strength analysis of composite laminates, determination of vibration modes and associated frequencies of tubular structures with anisotropic sandwich construction walls, and optimization of composite sandwich structures considering all of the above factors. The manufacturing technologies needed to build such a structure were also developed. These technologies included the building of co-cured honeycomb panels, curved panels, core splices, and tubular sections. These efforts culminated in the production of a space-worthy component.

Nomenclature

$\mathbf{A}$, $\mathbf{D}$	In-plane and bending stiffness matrices
E_l	Ply longitudinal modulus
E_t	Ply transverse modulus
G_{lt}	Ply shear modulus
h	Telescope tube thickness
L	Telescope tube length
LF_A	Quasi-static axial load factor
LF_L	Quasi-static lateral load factor
m^*	Mass per unit area of tube wall
M	Satellite mass
$\mathbf{M}$, $\mathbf{K}$	Mass and stiffness matrices
R	Median radius of telescope tube
S	Ply shear strength
t_{fc}	Facesheet thickness
t_c	Core thickness
T_1	Maximum structure temperature
T_2	Minimum structure temperature
T_0	Optical calibration temperature
u_0, v_0, w	Midplane displacements
x	Axial coordinate
X_t	Ply longitudinal tensile strength
X_c	Ply longitudinal compression strength
Y_t	Ply transverse tensile strength
Y_c	Ply transverse compression strength
α_l	Ply longitudinal CTE
α_t	Ply transverse CTE
α_x	Tube longitudinal CTE
β_x, β_θ	Midplane rotations
ΔL	Beam tip extension for thermal model
ΔT_{Ext}	Temperature change which induces extension
ΔT_{Bend}	Temperature change which induces bending
ΔY	Beam tip displacement for thermal model
ε_x^o, ε_θ^o, $\gamma_{x\theta}^o$	Midplane strains
ε_m, α_m	Beam mode constants
θ	Circumferential coordinate
Θ	Angular beam tip displacement for thermal model
κ_x^o, κ_θ^o, $\kappa_{x\theta}^o$	Midplane curvatures
ρ	Density
σ_{CTE}	Standard deviation of CTE
ν_{lt}	Ply major Poisson's ratio
φ_u, φ_v, φ_w	Beam vibration modes
ω	Natural frequency

* Class of 1943 Assistant Professor of Aeronautics and Astronautics, MIT
** Research Assistant, MIT
*** Principle Member of Technical Staff, Charles Stark Draper Laboratory

Introduction

Satellite structures must survive launch, meet outgassing and other mission specific requirements, provide stiffness, dimensional stability and thermal control, and allow equipment mounting and containment. Current design practice is to have separate structures for each of these functions. This practice is acceptable for large vehicles, but does not scale well. In small vehicles, many of these functions can be met with very little material, resulting in designs dominated by practical manufacturing constraints (minimum gages, tolerances, etc.) rather than the actual requirements. As a consequence, the true structural mass fraction (including things like electronics support racks and boards, radiators and thermal control material, and launch-related structures such as cradles and support frames for multiple vehicles) becomes very large in miniature vehicles. This presents a problem, but also an opportunity. In general, an examination of the basic physics that sizes such systems is very favorable to small systems. For example, the material stiffness required to achieve desired deflections and vibration frequencies increases in proportion to the structural size raised to the third power. However, for very small vehicles it is difficult to take advantage of the physics, because practical considerations such as minimum material gages, joining technology, and the need for equipment containment and support limit the use of current designs and design practices. New approaches for the design and integration of primary structure and hardware for functions such as thermal control and equipment mounting are needed.

A joint MIT/Draper Laboratories program is presently underway to meet these needs[1]. New technologies have been developed and demonstrated via the design and construction of a structure for a recently proposed small satellite. The proposed satellite is a small (1m by 0.5m, 50kg) earth observation satellite. The structure is multifunctional: it must provide support during launch, provide a stable platform for the optics of a reflecting telescope in orbit, and provide mounting points for solar cells, electronics, and numerous other components. The structure must be very stiff and compact to control launch loads and vibrations in orbit and to minimize the weight and complexity of the control system. To reduce cost, the structure should be versatile, not require special handling, and be easy to manufacture.

This paper describes the technologies developed and used to design and manufacture a multifunctional space structure. After an overview of the structure, all analytical techniques used will be reviewed and/or developed. The analyses are then used in two stages. First, system requirements are reduced to structural and material requirements via preliminary thermal, optical, and strength calculations. Then an optimum structure is designed using a shell analysis to determine global natural frequencies and an extended Classical Laminated Plate Theory (CLPT) to assure strength and thermal stability, combined with a newly developed optimization scheme. The development of manufacturing techniques is also described. Methods for cocuring one-piece tubular structure with sandwich construction walls with honeycomb cores and graphite/epoxy face sheets are covered. Finally, a design for the space-worthy structural component produced under the program is described.

Structural Geometry

A double shell design was chosen for the satellite. The structure consists of a inner tube surrounded by an octagonal outer structure. The structural configuration is illustrated in Figure 1.

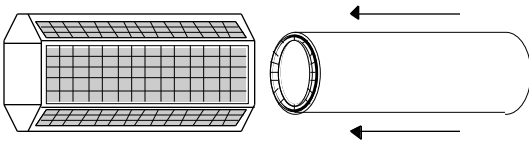

Solar Panel Structure Telescope Tube

Figure 1. Structural configuration

The inner structure is referred to as the telescope tube. The telescope tube is the primary load carrying structure. Figure 2 is a diagram showing the location of the components inside the telescope tube. The sensitive optics are housed inside the tube. Volume unused by the optics houses equipment for other major systems, such as attitude control, guidance, and navigation. The equipment is attached directly to the tube wall.

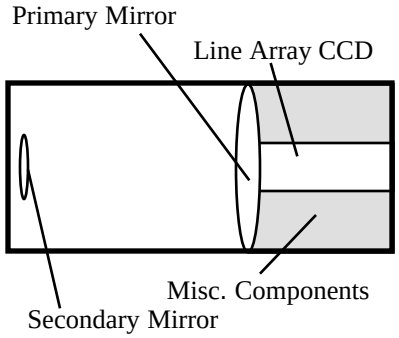

Figure 2. Internal component configuration

The telescope tube has a median diameter of 42.4 cm (16.75") and a length of 1 meter. The tube is composed of two 4 ply facesheets made of AS4/3501-6 graphite epoxy with a $[0/\pm 47/0]_T$ layup. Separating the face sheets is a 1.9 cm (0.75") thick low density aluminum honeycomb core.

The octagonal outer structure is named the solar panel structure. Its primary function is to provide flat surfaces for mounting solar cells. The solar panel structure also redistributes thermal loads around the telescope tube, and provides a location to directly attach electronics may be directly attached to the back of the panels between the telescope tube and solar panel structure. The solar panel structure will have an outer diameter of 50 cm, a length of 1 meter, and have a composite sandwich construction. This paper will concentrate on the design of the telescope tube. The design of the solar panel structure will be detailed in a future paper.

Analysis

Several analytical techniques were used in the development of the small satellite structure. An analysis technique was developed to determine the temperature distribution around the satellite while in orbit. This temperature distribution could then be used to determine the relative displacement of the optics. A ray tracing analysis was then used to determine the degradation in optical performance. From this analysis it is possible to determine an upper-bound on the Coefficient of Thermal Expansion (CTE) for a desired level of optical performance. A quasi-static analysis was performed to insure survival of the satellite during launch. Vibrational analysis was performed to maximize the fundamental frequency so that the structure appeared "rigid" to the control system. Finally these techniques were then used in a formal optimization code to determine the "best" structure design.

Thermal Analysis. The thermal response of a tubular structure in various orbital positions was determined using the analytical methods presented in References 2-4. Thermal loading conditions including solar, Earth emitted, and Earth reflected heating with the satellite in noon, sunrise, and midnight positions were considered. The steady state average temperature and temperature gradient (from one side of the structure to the other) were computed, as were a limited number of transient cases carried out over an entire orbit. The effects of internal radiation were considered parametrically. Results of the thermal analysis were expressed as two parameters, T_1, the maximum temperature, and T_2, the minimum temperature of the structure. For most orbital positions considered T_1 was the temperature of the structure facing the sun, and T_2 was the dark side temperature.

Thermal Deformation Model. The thermal states calculated using the thermal analysis were incorporated in a simple thermal deformation model to calculate (i) the change in length of the structure due to the change in the average temperature of the structure from the temperature at which the optics were calibrated, and (ii) the bending distortion of the structure, both length change and angle error, due to a temperature gradient from one side of the structure to the other. If the temperature gradients are assumed to be linear, deformations in both of these cases are stress-free, and can be calculated directly by integrating the thermal strains. The telescope tube can then be modeled as a beam to determine the deformations due to thermal loading.

Figure 3 shows a cantilevered beam which is subjected to two different temperatures on either side and the resulting deformation.

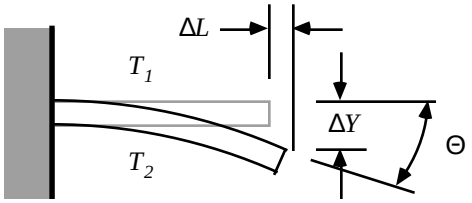

Figure 3. Beam subject to linear temperature gradient

If T_0 is the temperature at which the optics are calibrated, and $T_1 > T_2$, then the change in temperature on either side is given by:

$$\Delta T_1 = T_1 - T_0 \tag{1}$$

$$\Delta T_2 = T_2 - T_0 \tag{2}$$

These changes in temperature can be transformed into a change in temperature which causes extension and a change in temperature that causes bending of the beam:

$$\Delta T_{Ext} = \frac{\Delta T_1 + \Delta T_2}{2} = \frac{T_1 - T_2}{2} - T_0 \tag{3}$$

$$\Delta T_{Bend} = \Delta T_1 - \Delta T_2 = T_1 - T_2 \tag{4}$$

If the temperature gradients are assumed linear (i.e. the beam undergoes stress free deformation), and through thickness shear strains are neglected, then using only geometric considerations the thermal deformations can be found. The angular difference between the

midplane of the beam and the tip is then given by:

$$\Theta = \frac{L\alpha_x}{2R}\Delta T_{Bend} \quad (5)$$

Here, L is the length of the tube, R is the radius measured to the centerline of the tube wall, and α_x is the axial CTE of the tube wall. The displacement of the tip is given by:

$$\Delta Y = 2R\left(1-\mathrm{Cos}(\Theta)\right)\left(\frac{1+\alpha_x\Delta T_{Ext}}{\alpha_x\Delta T_{Bend}}\right) \quad (6)$$

The axial displacement of the beam is:

$$\Delta L = 2R\,\mathrm{Sin}(\Theta)\left(\frac{1+\alpha_x\Delta T_{Ext}}{2\alpha_x\Delta T_{Bend}}\right) - L \quad (7)$$

The above three equations do not assume small angle deformations. If it is assumed that the angular tip displacement is small then the following approximations can be made:

$$\Delta Y \approx \frac{L^2}{4R}\left(\alpha_x\Delta T_{Bend} + \alpha_x^2\Delta T_{Bend}\Delta T_{Ext}\right) \quad (8)$$

$$\Delta L \approx L\alpha_x\Delta T_{Ext} \quad (9)$$

The second term in equation 8 represents the extension-bending coupling. The coupling term proved to be inconsequential for the configurations considered. Neglecting this term reduces equations 8 and 9 to the familiar form describing the thermal deformation of beams. The analysis has been developed for a cantilevered structure; an unsupported (free-free) structure can be analyzed as two identical cantilevered structures by assuming symmetry about the centerline, and replacing L with $L/2$ in the equations above.

Optics Performance Model. One of the functions of the structure is to support telescope optics. The primary mirror is supported near the middle of the structure, and the secondary mirror supported at one end, as shown in Figure 2. The thermal deformations cause a change in distance and angular orientation between the two mirrors resulting in degradation in performance of the telescope. The calculation of the optical degradation was done at Draper Laboratories. For a given length change ΔL, and angular misalignment Θ, a ray tracing routine was used to calculate the Strehl number, a metric of the image quality[5]. A Strehl number of 1.0 represents a perfect telescope. A maximum Strehl number of 0.977 can be achieved with the desired aperture and focal length for this telescope assuming no misalignment of the mirrors due to deformation. A Strehl number of greater than 0.90 is required for this application.

Composite Computation. Existing models were used for the analysis of composite sandwich panels. Classical Laminated Plate Theory (CLPT)[6] was used to calculate effective sandwich panel properties from the properties of ply and core materials. Table 1 lists the properties for the material used for the face sheets, AS4/3501-6 graphite-epoxy. The material properties were gathered from existing references[7]. The core was modeled as having negligible properties in-plane; out-of-plane properties were taken from Reference 8. Thermal deformation properties and the effects of manufacturing and material variations were calculated by modified CLPT relations coupled with simple probabilistic analyses[9,10]. Mechanically and thermally induced microcracking was calculated using methods previously developed at the TELAC laboratory[11].

Structural Strength Calculations. Simple, conservative strength calculations were used for the design of the telescope tube. The structure was idealized as a cantilevered 1 m long 41 cm ID cylinder. A worst-case inertial loading corresponding to a single satellite in the launch vehicle was taken from the Pegasus Payload Users Guide[12], and was used to estimate the

Table 1. AS4/3501-6 Gr/E Material Properties

Property	Symbol	Value
Density	ρ	1820 Kg/m^3
Ply thickness	-	0.13 mm
Ply longitudinal modulus	E_l	142 GPa
Ply transverse modulus	E_t	9.81 GPa
Ply major Poisson's ratio	ν_{lt}	0.30
Ply shear modulus	G_{lt}	6.00 GPa
Ply longitudinal CTE	α_l	0.018 με/°C
Ply transverse CTE	α_t	28.8 με/°C
Ply longitudinal tensile strength	X_t	2356 MPa
Ply longitudinal compression strength	X_c	1468 MPa
Ply transverse tensile strength	Y_t	49.40 MPa
Ply transverse compression strength	Y_c	186.0 MPa
Ply shear strength	S	105.0 MPa

stress state. The structure was modeled as a thin-walled tube, ($h<<R$), cantilevered from a rigid support at one end. The tube wall consists of two identical facesheets of thickness t_{fc}, a core of thickness t_c, and a total thickness ($t_c + 2\ t_{fc}$) of h. The facesheets were assumed to carry all loads. The mass of the satellite (M) was assumed to be uniformly distributed on the structure. Quasi-static inertial loads were then applied. The average axial line load on the tube wall due to an axial inertial load is:

$$N_A = LF_A \frac{Mg}{2\pi R} \tag{10}$$

Where LF_A is a quasi-static axial load factor. The maximum axial line load due to a lateral inertial load is:

$$N_L = LF_L \frac{2MgL}{\pi\left(4R^2 + h^2\right)} \tag{11}$$

Where LF_L is a quasi-static lateral load factor. The line load N is the load per unit width on the tube wall. These loads were superimposed to find the maximum case loads. A factor of safety of 3.2 was used to account for stress concentrations and unintentional damage during handling. This was arrived at by multiplying a post impact compression strength factor of 2.3 by a design factor of safety of 1.4.

The worst-case loads were used in a Classical Laminated Plate Theory (CLPT) analysis of the tube wall. The stress in each ply of the composite were calculated and a Maximum Stress criteria was used to check for first ply failure.

Dynamic Behavior Model. A previously developed energy method for predicting the dynamic behavior of anisotropic tubes was extended[13]. The extended method can handle unbalanced laminates which exhibit twist-bend coupling. The method is used to determine the vibration modes and their associated frequencies.

The vibrations of the telescope tube were assumed to be representative of the vibration of the entire satellite. This was done primarily because the stiffness of the telescope tube is much greater than that of the solar panel structure. Therefore the telescope tubes' vibration modes will be independent of the vibration of the solar panel structure.

Using an assumed-mode energy method, the first natural frequency (fundamental frequency) of the telescope tube can be determined. Using Love's first approximation, the strain-displacement relations for a thin shell can be written as:

$$\begin{aligned}
\varepsilon_x &= \frac{\partial u_o}{\partial x} & \varepsilon_\theta &= \frac{1}{R}\left(\frac{\partial v_o}{\partial \theta} + w_o\right) \\
\gamma_{x\theta} &= \frac{\partial v_o}{\partial x} + \frac{1}{R}\frac{\partial u_o}{\partial \theta} & \kappa_x &= \frac{\partial \beta_x}{\partial x} \\
\kappa_\theta &= \frac{1}{R}\frac{\partial \beta_\theta}{\partial \theta} & \kappa_{x\theta} &= \frac{\partial \beta_\theta}{\partial x} + \frac{1}{R}\frac{\partial \beta_x}{\partial \theta} \\
\gamma_{xz} &= \beta_x + \frac{\partial w}{\partial x} & \gamma_{\theta z} &= \beta_\theta + \frac{1}{R}\left(\frac{\partial w}{\partial \theta} - v_o\right)
\end{aligned} \tag{12}$$

Where the subscript o refers to values at the shell midplane, and β_x and β_θ are the rotations in the x and θ directions respectively. Note that engineering notation is used for the shear strains. Assuming that out of plane shearing strains are zero, then the rotations can be solved for:

$$\beta_x = -\frac{\partial w}{\partial x} \qquad \beta_\theta = \frac{1}{R}\left(v_o - \frac{\partial w}{\partial \theta}\right) \tag{13}$$

These can then be substituted in to equation 12 to solve for the curvatures.

Cylinders exhibit two distinct types of vibrational modes: beam and shell modes. Free-free cylinders with large length-to-radius ratios behave as predicted by beam theory, thereby exhibiting beam modes. Beam modes are associated with in-plane deformations of the tube wall. Free-free cylinders with small length-to-radius ratios exhibit shell modes. Shell modes are the circumferential deformations of the cylinder, which are associated with bending deformations of the cylinder wall. Figure 4 and 5 illustrates the two modes for the free-free case.

Figure 4. Beam vibrational modes

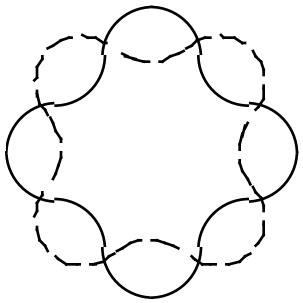

Figure 5. Circumferential vibration modes

Cantilevered cylinders with moderate *R/L* ratios exhibit both modes. The vibration mode associated with the fundamental frequency of such a cylinder is a combination of a beam mode and a shell mode; not necessarily the first of each. The fundamental frequency of the cylinder can involve, for example, the fifth shell mode and the first beam mode.

Based on the above, the displacement field for the cylinder is assumed to be separable functions of time, *t*, axial position, *x*, and circumferential angle, θ:

$$\begin{aligned} u_o &= \left\{ q_{u1}(t)\mathrm{Cos}(n\theta) + q_{u2}(t)\mathrm{Sin}(n\theta) \right\} \varphi_u(x) \\ v_o &= \left\{ q_{v1}(t)\mathrm{Cos}(n\theta) + q_{v2}(t)\mathrm{Sin}(n\theta) \right\} \varphi_v(x) \\ w &= \left\{ q_{w1}(t)\mathrm{Cos}(n\theta) + q_{w2}(t)\mathrm{Sin}(n\theta) \right\} \varphi_w(x) \end{aligned} \quad (14)$$

The cosine and sine terms govern the shell component of the cylinder, and *n* is the nth shell component. The beam mode shape φ will be determined later. For an orthotropic shell the strain energy can be written as:

$$U = \iint_A \begin{Bmatrix} \frac{1}{2}(A_{11}\varepsilon_x^{o\,2} + A_{22}\varepsilon_\theta^{o\,2} + A_{66}\gamma_{x\theta}^{o\,2} + \\ D_{11}\kappa_x^{\,2} + D_{22}\kappa_\theta^{\,2} + D_{66}\kappa_{x\theta}^{\,2}) + \\ A_{12}\varepsilon_x^{\,o}\varepsilon_\theta^{\,o} + D_{12}\kappa_x\kappa_\theta + \\ D_{16}\kappa_x\kappa_{x\theta} + D_{26}\kappa_\theta\kappa_{x\theta} \end{Bmatrix} Rd\theta\,dx \quad (15)$$

Here, the *A* and *D* values are components of the familiar CLPT **A** (in-plane stiffness) and **D** (bending stiffness) matrices. Neglecting the rotational inertial terms, the kinetic energy is given by:

$$T = \frac{m^*}{2}\iint_A \left\{ \left(\frac{\partial u_o}{\partial t}\right)^2 + \left(\frac{\partial v_o}{\partial t}\right)^2 + \left(\frac{\partial w}{\partial t}\right)^2 \right\} Rd\theta dx \quad (16)$$

The assumed displacements, equation 14, can be substituted into the strain-displacement relations, equations 12 and 13, to find the strains in terms of the separable functions. The strains and displacements can then be substituted into the definitions of potential and kinetic energy, equations 15 and 16. These are then substituted into Lagrange's equation to determine the response of the system in terms of the unknown modal amplitudes $\underline{q}$.

$$\mathbf{M}\ddot{\underline{q}}(t) + \mathbf{K}\underline{q}(t) = 0 \quad (17)$$

The above equations can be used to determine the vibrational modes of the system. **M** and **K** are 6 × 6 matrices with constant coefficients, expressed as integrals of the assumed displacements. If $\underline{q}(t)$ is assumed to be $\underline{q}_o e^{\lambda t}$ then equation 17 reduces to a simple eigenvalue problem.

Evaluation of **M** and **K** in equation 17 requires assumed mode shapes for the axial modes, φ. Four classes of these shapes will be considered. First, if the satellite is cantilevered inside the launch vehicle, one end will be clamped and the other end free. Clamped-free beam mode shapes can be assumed for the beam component shapes:

$$\varphi_u = \varepsilon_m \begin{Bmatrix} Sinh\left(\frac{\varepsilon_m x}{L}\right) + Sin\left(\frac{\varepsilon_m x}{L}\right) - \\ \alpha_m\left[Cosh\left(\frac{\varepsilon_m x}{L}\right) - Cos\left(\frac{\varepsilon_m x}{L}\right)\right] \end{Bmatrix} \quad (18)$$

$$\varphi_v = \varphi_w = Cosh\left(\frac{\varepsilon_m x}{L}\right) - Cos\left(\frac{\varepsilon_m x}{L}\right) - \alpha_m\left[Sinh\left(\frac{\varepsilon_m x}{L}\right) - Sin\left(\frac{\varepsilon_m x}{L}\right)\right]$$

Values of ε_m and α_m can be found tabulated in Reference 12 for three axial modes. The *m* subscript indicates the beam mode number. For the fundamental frequency *m* = 1.

Determining the vibrational characteristics of the cylinder in space is slightly harder. In the space environment the cylinder undergoes free-free vibration. There are three possible classes of mode shapes in this case. The first class is Rayleigh modes, illustrated in Figure 6.

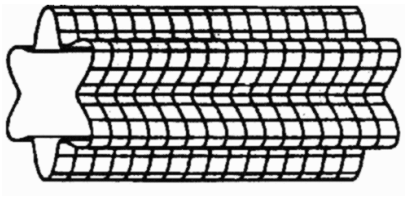

Figure 6. Rayleigh Mode (from Reference 14)

These are pure shell modes. Equation (19) gives the assumed axial mode shapes for the Rayleigh modes.

$$\begin{aligned} \varphi_u &= 0 \\ \varphi_v &= \varphi_w = 1 \end{aligned} \quad (19)$$

The second possible mode shape is the Love modes. Love modes are anti-symmetric about the midpoint of the cylinder. A Love mode is illustrated in Figure 7.

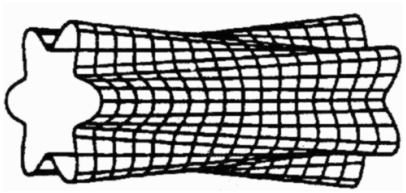

Figure 7. Love Mode (from Reference 14)

The mode shapes for the Love mode are given by:

$$\varphi_u = -1$$
$$\varphi_v = \varphi_w = \tfrac{1}{2} - x/L \qquad (20)$$

The third possible mode shape class utilizes the free-free beam modes:

$$\varphi_u = \varepsilon_m \left\{ \begin{array}{l} \left[\mathrm{Cosh}\left(\frac{\varepsilon_m x}{L}\right) + \mathrm{Cos}\left(\frac{\varepsilon_m x}{L}\right) \right] \\ \alpha_m \left[\mathrm{Sinh}\left(\frac{\varepsilon_m x}{L}\right) - \mathrm{Sin}\left(\frac{\varepsilon_m x}{L}\right) \right] \end{array} \right. \qquad (21)$$

$$\varphi_v = \varphi_w = \mathrm{Sinh}\left(\frac{\varepsilon_m x}{L}\right) - \mathrm{Sin}\left(\frac{\varepsilon_m x}{L}\right) - \alpha_m \left[\mathrm{Cosh}\left(\frac{\varepsilon_m x}{L}\right) - \mathrm{Cos}\left(\frac{\varepsilon_m x}{L}\right) \right]$$

This mode is excited when the circumferential stiffness is much greater than the axial stiffness.

Once the mode shapes are assumed, equation 17 is evaluated and solved for different combinations of modes until the fundamental frequency is found. It should be noted that assuming mode shapes will over-predict the frequency of the structure. This analysis will also over-predict the frequency due to the fact the shearing deformations are assumed to be zero. A Ritz analysis is currently under development to increase the accuracy of the predicted fundamental frequency.

Optimization. The very large number of possible designs for the structure, even after careful reduction of design variables, requires a formal optimization procedure to determine the best design. The method must be capable of handling some unusual criteria, such as minimizing the effects of manufacturing and material variations. A suitable method has been under development in a separate, ongoing project in the TELAC laboratory[15,16].

Requirements Analysis

A series of analyses were carried out to determine the structural requirements from the overall system requirements.

Thermal and Dimensional Stability. The thermal and thermal deformation analyses were used parametrically to generate deformation predictions for a variety of mission scenarios. These were used to isolate critical factors. For example, it was found that the circumferential conductivity of the structure had a relatively small impact on thermal deformations, while the thermal mass had a moderate effect, and CTE had a strong effect.

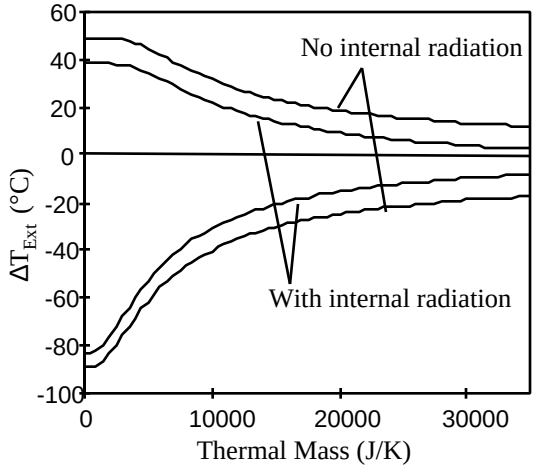

Figure 9. Transient extensional change in temperature versus thermal mass

Figure 9 shows the effect of the thermal mass of the structure on the maximum and minimum extensional temperatures seen in a typical orbit. In this analysis, the structure was assumed to be fully exposed to the environment; the external solar panel structure was not modeled. The cases of fully blocked or fully unimpeded internal radiation in the tube are shown. The above chart assumes a circumferential conductivity of 50 W/m K, which is very high for Gr/E. Other (steady state) analyses indicated that the thermal behavior of the structure is relatively insensitive to this parameter. Internal radiation can also be seen to be relatively unimportant. A typical design for the structure has a thermal mass of approximately 4500 J/K. In this case, the maximum and minimum transient extensional temperatures are +37 and -55 ^{o}C respectively for a calibration temperature of 20 ^{o}C.

A limited set of thermal deformation results were then used to calculate optical performances.

Again, critical factors were identified. It was found that the optical performance was dominated by the change in the structure's average temperature from the temperature at which the optics were calibrated. This change in temperature caused axial deformations that defocused the optics. Thermal gradients from one point in the structure to another had relatively small effects on performance. Figure 10 shows calculated Strehl numbers for a range of extensional and bending ΔT's, assuming a CTE of 0.18 με/°C, the minimum practical manufacturable CTE[10].

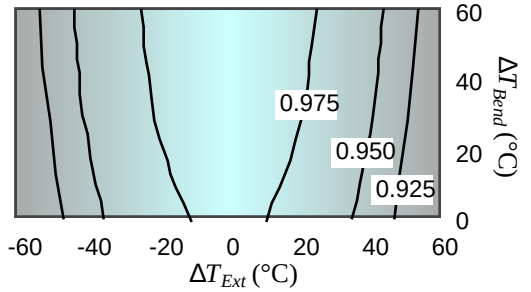

Figure 10: Strehl number versus temperature

From the figure it can be seen that bending deformations have less significant effects than the extensional deformations. The performance requirement is a Strehl number greater than 0.9. In the range of temperatures predicted for an unprotected structure, with a very low CTE assumed, the performance is marginal, and this does not consider other sources of error such as optics imperfections, alignment, jitter, etc. For this reason, it is clear that the tube axial CTE must be held as low as possible, and some means of protecting the tube from the direct effects of the environment is required.

Launch Survival. A Pegasus launch scenario from Reference 12 resulted in an equivalent quasi-static loading on the structure of 13.25 g's axially and 9.5 g's laterally. The axial loads on the tube wall where calculated using equations 10 and 11. All layups considered were subjected to the strength analysis, using these loads, to determine if failure of any kind would occur. A large factor of safety (FOS) of (3.2) was applied to account for the possibility of both stress concentrations at structural details and unintentional damage during handling. It was found that all practical designs had very high margins of safety, and hence strength was not further considered as a design driver. For example, the design selected had a margin of safety of 13.0 against first ply failure.

Stiffness and Mass. It was determined in cooperation with Draper Lab personnel that major increases in performance and/or simplification of control and pointing systems could be accomplished by a very high structural stiffness. This was also desirable to minimize jitter in orbit and acoustic excitation during launch. These advantages were difficult to quantify at the level of detail of system design available, but it was agreed that a target first natural frequency of 90-100 Hz. was desirable, and this was adopted as a target for the structure. The complexity of the tube vibration behavior did not allow this requirement to be reduced to a simple structural parameter such as tube wall thickness or modulus. The mass requirement was also difficult to quantify at the level of detail of system design available. A firm requirement for structural mass was set to a rather generous 10kg, but there it was determined that there are large advantages in reducing the weight as much as possible.

A summery of the requirements is given in Table 2. System requirements are listed along with derived structural requirements.

Design

The analysis techniques developed were used to find designs that met all requirements while minimizing weight and manufacturing complexity.

Configuration Trade. Several basic structural configurations were considered. Figure 11 illustrates the three basic designs selected.

Table 2. Requirements

Requirement	Symbol	Value
Minimum Strehl number		0.90
Minimize CTE		*≈0.0*
Quasi-static axial load factor	LF_A	13.25
Quasi-static lateral load factor	LF_L	9.5
Design axial load	N_X	*21.2 kN/m*
Robust, modifiable structure		
High design FOS		*3.2*
Fundamental frequency goal	-	90 - 100 Hz.
Design to meet it		
Mass target	*M*	<50 kg
Minimize structural mass		*10 kg or less*

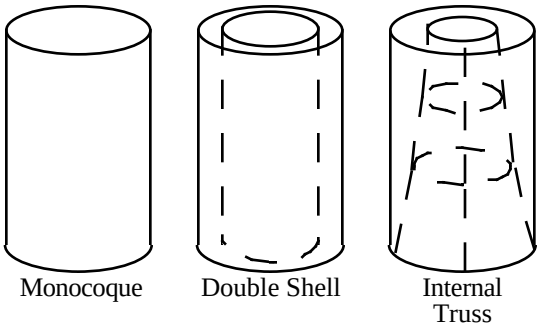

Figure 11. Candidate structural configurations

The first design is a monocoque design. A tubular structure would be used to meet all the thermal, vibrational and launch requirements. The thermal-structural-optical analysis showed that an unacceptable amount of optical degradation would occur for a single tubular structure attempting to meet the desired dimensions and nominal properties. A structure could not be feasibly constructed to counteract the deformations due to thermal loading. To reduce the thermal gradients a "double shell" structure was then proposed. The double shell structure would have a division of load carrying capability. The inner structure would be a tube which would carry the launch loads and maintain pointing of the telescope. The outer structure would also be tubular but would carry no load. It would act to redistribute the temperature around the inner structure. This structure design has one major drawback: a mass penalty is paid for the second structure. An internal truss structure was proposed in an attempt to decrease the mass of the satellite. This structural design would have an outer structure to redistribute the temperature, but would have a truss structure to maintain alignment of the optics. It was felt that a low CTE truss structure would be difficult to build. The primary problem would be designing zero CTE joints. Based on considerations of thermal shielding, manufacturing simplicity, cost, and modularity, a double shell configuration was selected. It consists of a tubular bus and optics support structure surrounded by an octagonal arrangement of flat panels which support solar cells on the outside and electronic components on the inside.

Material Selection. Hercules prepreg graphite epoxy system AS4/3501-6 was selected as the primary structural material. Hexel "flexcore" 65.68 kg/m^3 (4.1 lbs/in^3) 5052 aluminum honeycomb, and Cytec FM-300-M film adhesive were also selected. All of these decisions were based primarily on availability, cost and processability rather than performance advantages. Both the analysis and manufacturing techniques could be used on other materials as necessary if a more advanced, more expensive, but higher-performance structure was desired.

Laminate Trade Study. The dynamic behavior analysis revealed some very interesting design trade-offs between honeycomb core thickness, face sheet laminates, and weight. Thin-walled structures (the extreme example being ones without a honeycomb core at all) are dominated by their flexibility in local bending. Thickening the walls by using sandwich construction adds weight, but increases the bending stiffness of the tube wall, suppressing local bending and forcing the tube to vibrate in modes dominated by bending of the entire structure. Figure 12 shows an example of such a trade, for a cantilevered structure with $[0/\pm47/0]_T$ facesheets. As the core thickness is increased, the mode shape that the fundamental frequency is associated switches twice. For low thickness, local bending of the tube wall dominates (e.g. Figure 5); for high thicknesses, in-plane deformation of the wall leads to bending of the entire tube as a beam (e.g. Figure 4). Once the in-plane modes have been forced, further thickening of the honeycomb results in a negligible addition to the fundamental frequency. From these analyses, a core thickness of 1.9 cm (0.75") was found to be optimal.

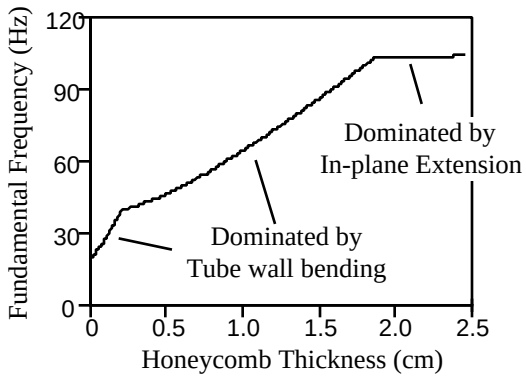

Figure 12. Clamped-Free fundamental frequency versus honeycomb thickness

Further decreases in natural frequencies can be achieved by maximizing the stiffnesses of the face sheets. It was found that acceptable stiffnesses could be achieved with sandwiches consisting of 4-ply facesheets bonded to the aforementioned 1.9 cm (0.75") core. The choice of laminates for the face sheets is constrained by the very severe requirement that the CTE of the face sheets be as low as possible. An analysis[10] considering the effects of manufacturing and material property variations on CTE showed that, for typical manufacturing variations (5% coefficient of variation in material properties and a 2 degree standard deviation in the ply angles), the lowest standard deviation on a practical zero CTE layup was about $\sigma_{CTE} \approx 0.18$ με/°C.

Facesheet Optimization. To optimize the in-plane properties, the tube wall was analyzed absent the core (which was assumed to have negligible properites in plane). It was found that 120 $[\pm\alpha/\pm\beta]_s$ balanced symmetric 8-ply laminates (considering only AS4/3501-6 material and integer layup angles) would meet the near zero CTE requirement. Symmetric laminates were selected to eliminate thermal bending of the structure when it is subjected to a uniform temperature. Balanced laminates were exclusively considered because there is no twisting of the structure when subjected to a uniform temperature. An optimization procedure was therefore developed that considered CTE, it's variation with expected material and manufacturing variation, and structural natural frequency (assuming a constant 0.75" core). Around 80 "acceptable" laminates were found. From these, a novel optimization procedure was used to find the best layup, which consisted of facesheets of $[0/+-47/0]_T$ on one side, and $[0/-+47/0]_T$ on the other[1].

Manufacturing

Tooling. An aluminum mandrel 40.6 cm (16") in diameter and 1.4 m (4.5 feet) long was prepared. A stock aluminum tube was surface finished, and end fixtures were attached. The fixturing was compatible with both an existing motorized rig for rotating tubes to aid in hand layups, and existing carts and fixtures for moving the rig into a large autoclave. Vacuum ports were also installed into the tube for autoclave curing. Additional fixturing for curing included a thin, flexible aluminum plate that served as the outer mold surface, and aluminum dams that defined the ends of the tube under construction.

Manufacturing Experiments. To confidently develop manufacturing methods, a series of manufacturing experiments were carried out. Flat plates, curved panels, rings, and partial tubes were built, each incorporating progressively more structural detail. Details included cocured sandwich construction; splices both in the straight and the curved directions, in both the honeycomb and the face sheets; difficulties associated with making closed (ring) sections; and mechanisms for releasing the mandrel from under the closed ring and tube sections.

Difficulties encountered and overcome in this process included core crushing due to autoclave pressure being applied to the sides of the honeycomb; dimpling and delaminations of the face sheets; face sheet wrinkling; poor splice bonding in the honeycomb core; mold lines from the outer mold surface; maintenance of face sheet alignments; and release of closed sections from the mandril. These problems were overcome by careful design of dams, systematic exploration of temperature and pressure cycles, careful use of an aluminum sheet as an outer mold surface, clipping together the core sections before cure; development of procedures for placement of face sheet plies, and use of teflon release material and a clamping apparatus to apply even force to the completed tube to remove it from the mandril[1].

Manufacturing Procedure. A one-piece, one-cure method for producing the composite tubes was finalized. Multiple layers of Teflon cloth were attached to the mandrel. The inner face sheet was built up on top of these. The necessary splices between the face sheet plies were staggered to avoid weak spots. It should be noted that no fibers were cut in the circumfrential direction, therefore all the plies were joined with matrix joints. The core was attached by film adhesive to the inner face sheet. The core material was spliced using aluminum clips to mechanically hold the core in place during cure, and a foaming adhesive placed down the length of the seams to mechanically bond them. The top face sheets were laid on top of another layer of film adhesive on the core. The entire structure was then vacuum bagged, and cured in an autoclave at 350°F for two hours. Figure 12 illustrates the cure cycle used; note the deliberate lack of a "flow" hold before proceeding to the cure temperature. This was omitted in an attempt to minimize dimpling.

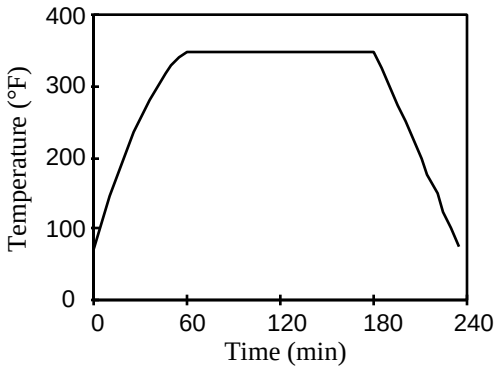

Figure 12. Cure cycle

The composite, the film adhesive holding the face sheets to the core, and the foaming adhesive bonding the core splices, were all simultaneously cured. During cure, full vacuum and an overpressure of 10 psi were applied. After cure, the structure and mandrel were allowed to cool to room temperature and the layers of Teflon pulled out from underneath the structure. This allowed the structure to be removed from the mandril without damage.

Structure Built. To date, a single full sized structure, a tube one meter long and 0.41 meters

in diameter, has been built. The walls are constructed of AS4/3501-6 graphite epoxy face sheets with layups of $[0/+-47/0]_T$ on one side, and $[0/-+47/0]_T$ on the other, bonded with FM-300M film adhesive to a flexcore very low density aluminum honeycomb core 0.75" thick. It weights approximately 5.5 kg. The quality of the tube appears to be very good, with only a few wrinkles or other defects visually evident. The construction required two days of labor from a crew of three relatively inexperienced workers, four hours of autoclave time, and approximately $500 in materials.

Conclusions

Structures for mini- and micro-satellites cannot be efficiently designed using techniques developed for larger vehicles. New design concepts, including multifunctional structures, promise to not only solve this problem, but deliver dramatic weight and cost savings and simpler and more reliable systems. Such structures have the combined capability to handle launch loading, on-orbit stiffness and dimensional stability, equipment containment and mounting, thermal control, and other requirements simultaneously, without the need for separate structures or systems.

This program has successfully developed and demonstrated the technology necessary for the design and production of multifunctional structures for typical small satellites. The experience gained in a complete design-build cycle has shown that the levels of both analytical and tooling work are reasonable, and it appears that the finished structures can be build with very low unit costs. The technology has been demonstrated for a specific application, but should be adaptable to others.

Some specific technical lessons have been learned. At least for the system considered here, strength requirements are easily met, thanks primarily to the physics that scale the problem. The same physics allows ultra-stiff structures, which are not practical on larger vehicles. Such structures will both increase performance, and allow lower complexity and cost in the control systems. The most demanding requirements are those of the optical systems, particularly the requirement that thermal distortions be kept extremely low without resorting to active thermal control. This requires very low CTE materials, and drives both the design process, which is limited to near-zero CTE layups, and the manufacturing, which must be high enough quality that manufacturing errors do not drive the CTE too far off the design point. More generally, the program has developed a procedure for the preliminary analysis of small satellite structures that should be adaptable to a range of missions.

Some interesting work has "spun off" from this project. An simple, fast analytical technique has been developed for analyzing the free vibrations of anisotropic honeycomb sandwich wall tubes. Results from this analysis show behavior of interest to designers of such structures. The thickness of the core controls the local bending stiffness of the walls and hence the circumferential vibration modes; the axial stiffness of the facesheets controls the overall bending modes of the structure. This observation allows a fairly straightforward design approach to be taken to these complex structures. This project has also used, and contributed to, technology under development in the TELAC laboratory in the areas of ultra-low CTE laminates[9-11], and multifunctional laminate optimization in the presence of material and manufacturing uncertainty.[14,15]

Future Work

This technology will be further developed through experimental verification, construction of additional hardware, and refinements of the analytical techniques developed.

The validity of the analytical techniques and the quality of the manufacturing will be verified experimentally. Laminate strength and stiffness will be checked through tensile and bending tests. Both coupons and beams made from the same cocured honeycomb sandwich as the full-sized structure will be tested. Structural stiffness and damping will be checked through dynamic vibration and "tap" tests of beam and tube structures. The CTE will be verified through dilatometer testing. Samples will also be exposed to simulated space thermal cycling, and both microscopic examination of damage, and testing for strength and stiffness after exposure, will be carried out.

MIT will also design and construct additional hardware, possibly including: 1) solar cell mounting panels; 2) bulkhead structures to attach the solar cell mounts to the telescope tube; 3) "hardpoint" hardware to attach arbitrary objects that would apply a concentrated load to the structure; and 4) "spider" structure to mount the secondary mirrors of an existing optical test system to the structure. Additional manufacturing experimentation will be performed to perfect the economical production of high quality structures.

The analytical techniques developed here will be enhanced to increase their accuracy and address some known weaknesses. The thermal analyses will be updated to account for the necessary

passive thermal shielding that will be provided by the solar panel structure. The stress free assumption on the thermal-structural analysis will be lifted, and a thermal analysis using a Ritz solution or FEM model will be performed on the satellite. Finite element analyses will be performed to verify the simplified analyses performed here, and assess the effects of core shear on the vibration behavior and stress concentrations and fitting designs on the strength.

Acknowledgment

This work was supported by the Charles Stark Draper Laboratory, Inc. under IR&D contract DL-H-484763.

References

1. Dunn, C. T., "Multifunctional Structures for Mini- and Micro-Satellites", Master's Thesis, Massachusetts Institute of Technology, Cambridge, MA, expected May 1997.
2. Thornton, E.A. and Kim, Y.A., "Thermally Induced Bending Vibrations of a Flexible Rolled-Up Solar Array," Journal of Spacecraft and Rockets, Vol. 30, No.4, July-Aug. 1993, pp. 438-448.
3. Kim, Y.A., "Transient Thermo-Structural Analysis of an Insulated Space Structure," Master's Thesis, Massachusetts Institute of Technology, Cambridge, MA, June 1994.
4. Kim, Y. A., and McManus, H. L., "Transient Thermal-Structural Response of a Space Structure with Thermal Control Materials", in *Aerospace Thermal Structures and Materials for a New Era, AIAA Progress in Aeronautics and Astronautics Series Vol. 168*, AIAA, Washington DC, 1995, pp. 96-115.
5. G. Cappiello, Draper IOM #E33-95-163, rev 1, August 31, 1995.
6. Jones, R. M., *Mechanics of Composite Materials*, Hemisphere, 1975.
7. Sawicki, A. J., "Damage Tolerance of Integrally Stiffened Composite Plates and Cylinders", Master's Thesis, Massachusetts Institute of Technology, Cambridge, MA, 1990.
8. Hexel Aluminum Flex-Core Data Sheet 2700, Sept. 1995.
9. McManus, H. L., "Probabilistic Methods for the Calculation of Laminate Properties", *Journal of Reinforced Plastics and Composites*, Vol. 12, June 1993, pp. 712-722.
10. McManus, H. L., and Abernathy, E., "Effects of Material and Manufacturing Variations on Dimensionally Stable Composite Structure", *Journal of Reinforced Plastics and Composites*, in press.
11. McManus, H. L. and Maddocks, J. R., "On Microcracking in Composite Laminates under Thermal and Mechanical Loading", *Polymers and Polymer Composites*, in press.
12. "Pegasus Payload User's Guide", Release COML-3.00, Orbital Sciences Corporation, Oct. 1993.
13. Resnick, B. S., "Effects of Orthotropicity, Boundary Conditions, and Eccentricity on the Vibrations of Cylindrical Shells", Master's Thesis, Massachusetts Institute of Technology, Cambridge, MA, 1966.
14. Vinson, J. R., *The Behavior of Shells Composed of Isotropic and Composite Materials*, Kluwer Academic Publishers, Dordrecht, The Netherlands, 1993.
15. Southard, B. M., and McManus, H. L., "Paths to Failure and Variability of Failure Loads of Composite Laminates", 37th AIAA/ASME/ASCE/AHS/ASC Structures, Structural Dynamics, and Materials Conference, Salt Lake City, UT, April 1996.
16. Southard, B. M., "On The Variability of Composite Laminate Properties: Prediction and Minimization", Master's Thesis, Massachusetts Institute of Technology, Cambridge, MA, expected Aug. 96.

HUGH L. N. MCMANUS

Class of 1943 Assistant Professor of Aeronautics and Astronautics,
Massachusetts Institute of Technology

Mr. McManus is the Class of 1943 Career Development Professor of Aeronautics and Astronautics at the Massachusetts Institute of Technology. His work centers on the application of advanced materials in realistic aerospace environments. Current work includes predicting the response of materials to extreme thermal environments, aging and microcracking of composites in high speed aircraft and space applications, damage tolerance and failure mechanisms of aircraft composites, design of low weight materials and structures for high temperature capability and extreme dimensional stability, and design of multifunctional space structures. Previously, Mr. McManus was a Structures Engineer at the Lockheed Missiles and Space Co., Space Systems Division. There, he participated in the analysis and design of space structures and rocket motors, the analysis of thermal deformation of structures and the development of advanced composite materials for use in space structures, survivable structures, and rocket motors. He has also worked with Kaman AviDyne as a Research Engineer, working on analysis and design of aerospace systems for severe thermal environments. Mr. McManus received a Ph.D. degree in Mechanical Engineering from Stanford University in 1990, and S. B. and S. M. degrees in Aeronautical and Astronautical Engineering from MIT in 1980 and 1981. He is a senior member of the American Institute of Aeronautics and Astronautics, advises the MIT student branch, and has served on the Structures Technical Committee, chairing the Thermal Structures Subcommittee. He was a member of the National Research Council Committee on Reusable Launch Vehicle Technology Development and Test Program, serves on the ASTM Committee D-30 on High Modulus Fibers and Their Composites, and is a member of the Society of Advanced Materials and Process Engineers and Tau Beta Pi. He was the Boeing Career Development Professor for 1990-94, was an ASEE Faculty Fellow for 1992-93, and was named an NSF Young Investigator Award winner in 1992.

CHRISTOPHER T. DUNN

Research Assistant, Massachusetts Institute of Technology

Christopher T. Dunn is a Master's degree candidate at the Massachusetts Institute of Technology. He is working the Technology Laboratory for Advanced Composites, TELAC, in the material and structures division of the Aeronautics and Astronautics department. Christopher started his candidacy in June, 1996, and is currently a Draper Fellow, designing multifunctional structures for small satellites. He received a B.S. degree in Aerospace Engineering from the Pennsylvania State University in May 1996. While at Penn State he led the structural design team for the Penn State/Martin Marietta Get Away Special Project.

MICHAEL SOCHA

Principle Member of Technical Staff, Charles Stark Draper Laboratory